

FOCUS on Contamination: A Geospatial Deep Learning Framework with a Noise-Aware Loss for Surface Water PFAS Prediction

Jowaria Khan¹, Alexa Friedman², Sydney Evans², Runzi Wang³, Kaley Beins², David Andrews² and Elizabeth Bondi-Kelly¹

¹University of Michigan, Ann Arbor

²Environmental Working Group

³University of California, Davis

jowaria@umich.edu, {alex.friedman, sydney.evans}@ewg.org, mrrwang@ucdavis.edu, {kaley.beins, dandrews}@ewg.org, ecbk@umich.edu

Abstract

Per- and polyfluoroalkyl substances (PFAS), chemicals found in products like non-stick cookware, are unfortunately persistent environmental pollutants with severe health risks. Accurately mapping PFAS contamination is crucial for guiding targeted remediation efforts and protecting public and environmental health, yet detection across large regions remains challenging due to the cost of testing and the difficulty of simulating their spread. In this work, we introduce **FOCUS**, a geospatial deep learning framework with a label noise-aware loss function, to predict PFAS contamination in surface water over large regions. By integrating hydrological flow data, land cover information, and proximity to known PFAS sources, our approach leverages both spatial and environmental context to improve prediction accuracy. We evaluate the performance of our approach through extensive ablation studies and comparative analyses against baselines like sparse segmentation, as well as existing scientific methods, including Kriging and pollutant transport simulations. Results highlight our framework’s potential for scalable PFAS monitoring.

1 Introduction

PFAS or per- and polyfluoroalkyl substances are persistent “forever chemicals” widely used in industrial and consumer products such as non-stick cookware, waterproof textiles, and firefighting foams. Unfortunately, these substances resist degradation and accumulate in water, soil, and living organisms, with 97% of Americans exhibiting detectable levels in their blood [CDC, 2024]. Such pervasive exposure is linked to severe health risks including cancers, liver damage, and developmental disorders [Manz, 2024].

Although PFAS contamination is widespread and present in surface water [Langenbach and Wilson, 2021], groundwater [Schroeder *et al.*, 2021], and soil [Crone *et al.*, 2019], the high cost of sampling has resulted in sparse ground truth data, leaving us uncertain about where the highest concentrations

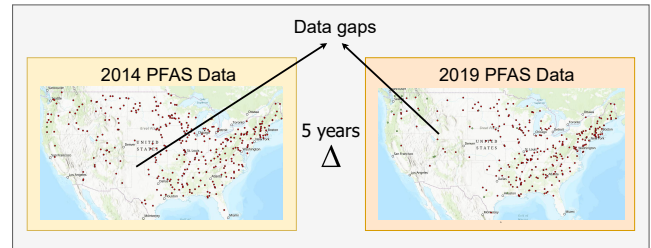


Figure 1: Challenges in generating PFAS contamination maps [U.S. EPA, OW, 2015]

occur. This lack of detailed spatial information hampers targeted remediation and calls for scalable, data-driven methods to identify PFAS hotspots and safeguard drinking water.

Artificial intelligence (AI) presents a promising avenue for addressing complex health and environmental issues, including identifying PFAS hotspots. In various domains, AI has proven effective at automating labor-intensive tasks and synthesizing domain expertise, whether in land cover mapping [Robinson *et al.*, 2020], agricultural optimization [Kerner *et al.*, 2024], or disease prediction [Bondi-Kelly *et al.*, 2023]. In the domain of PFAS contamination prediction, scientists have predominantly applied machine learning (ML) models such as random forests [Breiman, 2001] and XGBoost [Chen and Guestrin, 2016]. For example, [DeLuca *et al.*, 2023] used a Random Forest model to predict PFAS contamination in the Columbia River Basin via a tabular approach that aggregates environmental features within a 5 km buffer around sample points, which helps account for the limited ground truth data.

Building on these efforts, we frame PFAS prediction as a geospatial deep learning (DL) task. Our approach directly processes imagery, preserving spatial dependencies and reducing the need for extensive feature engineering, leading to more efficiency. This approach will also allow for repeated, high-resolution mapping to support ongoing monitoring efforts.

Our contributions in this work are summarized as follows:

- We propose **FOCUS** (**F**ramework for **E**nvironmental **C**ontamination with **U**ncertainty **S**caling), a framework employing a geospatial DL model for segmentation

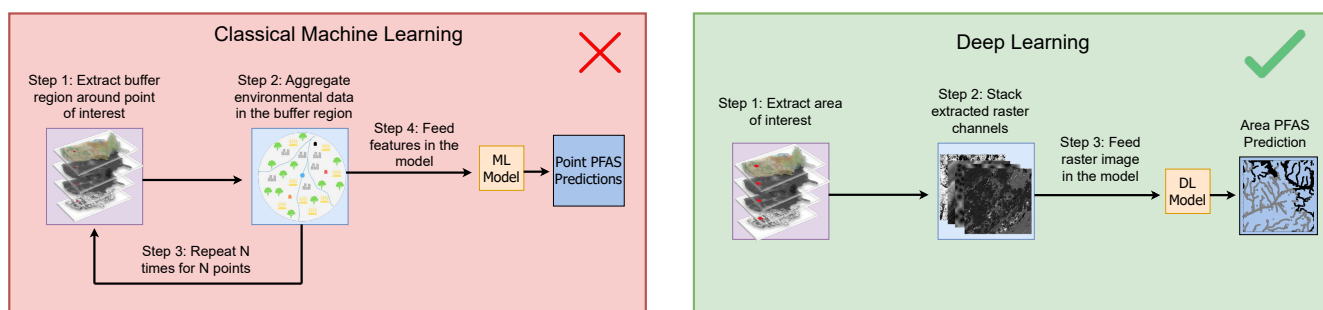


Figure 2: Left: Classical ML techniques aggregate surrounding pixel data to predict contamination at specific points; Right: DL methods process raster images directly to generate dense PFAS contamination maps in a single pass.

of PFAS contamination using rasters (e.g., grid-based geospatial data like satellite imagery or elevation maps).

- Our framework features a novel noise-aware loss that leverages domain expertise on PFAS spread to automatically fill data gaps and weight these assumptions by confidence, thereby addressing the challenge of limited labeled data.
- We benchmark our sparse segmentation framework against other AI models, [DeLuca *et al.*, 2023], and popular methods like simulations inspired by Soil and Water Assessment Tool (SWAT) [SWAT, nd] and Kriging [GISGeography, 2017], demonstrating our framework’s scalability, accuracy, and robustness for large-scale PFAS prediction.
- Through ablation studies, we assess our FOCUS loss function and hyperparameter selection.

We develop this framework together with a nonprofit organization actively working on environmental research, and an academic researcher specializing in water quality models, ensuring that our approach is grounded in the latest expertise and real-world environmental concerns.

2 Related Work

The study of PFAS contamination has gained significant attention due to its widespread environmental and health impacts. Existing research in this domain spans analytical methods from scientific domains for detecting and understanding contamination patterns, as well as emerging computational approaches, including AI techniques, aimed at improving detection and prediction capabilities.

Current Ways to Measure and Predict PFAS. The measurement of PFAS relies on laboratory-based analysis of water, fish tissue, and human blood samples with techniques such as liquid chromatography-tandem mass spectrometry (LC-MS) [Shoemaker and Tettenhorst, 2020]. Fish accumulate PFAS over time, serving as integrative indicators of water contamination hotspots that may be missed by sporadic water sampling. Therefore, fish tissue measurements provide complementary, long-term insights into PFAS presence, as well as potential exposure risks to anglers [Environmental Working Group, 2023]. While highly accurate, these methods are

costly [Doudrick, 2024], time-intensive, and difficult to scale for large spatial datasets.

PFAS monitoring efforts have made use of such measurement techniques and beyond. For example, states such as Colorado have implemented water testing, treatment grants, and regulatory measures since 2016 [Colorado Department of Public Health and Environment, nd]. In addition, there are community-based water sampling initiatives such as volunteer sampling by the Sierra Club [Sierra Club, nd] and focused efforts by organizations like the Ecology Center [Eco-Center, nd]. A recent study further underscores the importance of these efforts, revealing associations between PFAS contamination in drinking water and higher COVID-19 mortality rates in the U.S. [Liddie *et al.*, 2024]. Resources like the PFAS-Tox Database [Pelch *et al.*, 2022] further assist researchers, policymakers, and communities in monitoring PFAS. These efforts are important and complementary to FOCUS; we aim to bridge critical data gaps and provide continuous, scalable predictions until additional sampling can be carried out.

Various modeling approaches have been explored to predict contaminant distribution. Hydrological models such as SWAT [SWAT, nd] and MODFLOW [ktorcoletti, 2012] simulate pollutant transport using environmental parameters like flow rates, land use, and weather conditions. While effective, these models require extensive data and are computationally expensive at large scales [Zhi *et al.*, 2024]. Kriging, a geostatistical interpolation technique, has been widely used for mapping pollutants, including soil contamination [Largueche, 2006] and groundwater quality estimation [Singh and Verma, 2019]. Though useful in data-sparse environments, Kriging relies on simplifying assumptions such as spatial continuity and stationarity [GISGeography, 2017] that may not hold for complex contaminants like PFAS, whose transport dynamics and uncertainties are more intricate. We aim to take a data-driven, expert-informed approach to address these challenges.

AI Approaches for PFAS Prediction. Recent advances in AI and geospatial modeling have opened new avenues for tackling the complexities of PFAS detection and prediction by integrating environmental variables such as land cover, proximity to industrial facilities, and hydrological flow patterns. For example, DeLuca *et al.* [DeLuca *et al.*, 2023] used random forests to predict PFAS contamination in fish tissue in the Columbia River Basin, leveraging geospatial data from

industrial and military facilities, while Salvatore *et al.* [Salvatore *et al.*, 2022] developed a “presumptive contamination” model based on PFAS-producing or -using facilities’ proximity in the absence of comprehensive testing data. On a national scale, the USGS applied XGBoost to forecast PFAS occurrence in groundwater [Tokranov *et al.*, 2023]. This model integrated explanatory variables such as PFAS sources, groundwater recharge, etc. to predict contamination in unmonitored areas leveraging precomputed rasters of these variables. Such approaches require extensive manual feature engineering, such as calculating buffer statistics for raster grid cells to generate precomputed rasters. This preprocessing is resource-intensive, and once complete, the model is applied to each raster cell individually, which can limit its ability to retain spatial context and dependencies.

Geospatial Models. Recent advances in geospatial deep learning have introduced foundation models trained on large-scale satellite datasets for improved spatial prediction. Models like Prithvi [Blumenfeld, 2023] and SatMAE [Cong *et al.*, 2023] use masked autoencoders (MAE) to learn generalizable spatial representations in a semi-supervised manner, leveraging both labeled and unlabeled data. Unlike some traditional ML approaches that require extensive feature engineering, these models process raster data directly, preserving spatial dependencies. However, many of these models assume that key environmental information is directly observable in satellite imagery. In contrast, PFAS contamination is not directly visible, necessitating the use of intermediate geospatial data products, such as land cover, to capture the underlying environmental processes. These models’ success in tasks like flood mapping and wildfire detection [Blumenfeld, 2023] suggests that, with the appropriate data preprocessing, they can leverage broad spatial context for PFAS prediction while minimizing manual effort.

Addressing Data Scarcity. In environmental data analysis, limited ground truth often necessitates pseudo- or augmented labels, which can introduce noise and lead to overfitting. Various strategies have been proposed to mitigate these issues, including label smoothing and robust loss functions (e.g., Huber loss [Gokcesu and Gokcesu, 2021], Generalized Cross-Entropy [Zhang and Sabuncu, 2018], bootstrapping loss [Reed *et al.*, 2015]), and focal loss [Lin *et al.*, 2018]). Weakly supervised methods like the FESTA loss [Hua *et al.*, 2022] further aim to capture spatial and feature relationships. Notably, FESTA is one of the closest approaches to ours, as it is specifically designed for segmentation of remote sensing images using sparse annotations. However, we hypothesize that such methods are less suitable for PFAS contamination mapping, as these approaches often assume spatial continuity, whereas the diffuse nature of contamination lacks clear object boundaries. We compare with FESTA to test this hypothesis (see Section 3.7). Moreover, while transfer learning and active learning [Li *et al.*, 2024] can help leverage sparse data, transfer learning is limited by our incomplete understanding of PFAS-specific hydrological processes, and active learning is highly dependent on the quality of uncertainty measures, which in complex environmental settings may require significant domain expertise. These challenges underscore the

need for methods that integrate domain-specific knowledge directly into the training process.

3 Methodology

3.1 Dataset

This study aims to perform segmentation on surface water pixels, classifying them as having PFAS concentrations above or below established health advisory thresholds using geospatial data. The dataset is built from the U.S. Environmental Protection Agency (EPA) National Rivers and Streams Assessment (NRSA) [U.S. EPA, OW, 2015] and the Great Lakes Human Health Fish Fillet Tissue Study [U.S. EPA, 2024b], which together provide 866 sample points collected over multiple years. PFAS concentrations in fish tissue were measured as continuous values in these datasets but were then categorized into above (1) or below (0) health advisory thresholds based on thresholds defined by the U.S. EPA’s Fish and Shellfish Advisory Program [U.S. EPA, 2024a]. These thresholds indicate the health risks associated with different PFAS compounds in fish tissue. These sample points also exhibit a significant class imbalance, with 775 points labeled as above (89.5%) and 91 labeled as below (10.5%) safety thresholds.

Our dataset consists of ground truth masks generated from these data, multi-channel raster images as features, and noise masks, all of which provide a spatially and environmentally contextualized representation of contamination risks.

3.2 Raster Image Generation

To spatially integrate the data, multi-channel raster images with 45 channels were generated around each sample point. Each image is a $P \times P$ pixels patch with a 30-meter resolution, centered on the geographic coordinates of the sample point, where the optimal value of P is determined in Section 3.8. These raster images integrate several key features. First, we incorporate readily available data products such as the National Land Cover Database (NLCD) raster [U.S. Geological Survey, 2024] to represent land cover types, and flow direction rasters that capture hydrological connectivity. In addition, we generate distance rasters to quantify proximity to potential PFAS dischargers. The discharger location data are obtained from the U.S. EPA Enforcement and Compliance History Online (ECHO) [U.S. Environmental Protection Agency, nd] and converted into distance rasters using a distance transform for efficient spatial analysis.

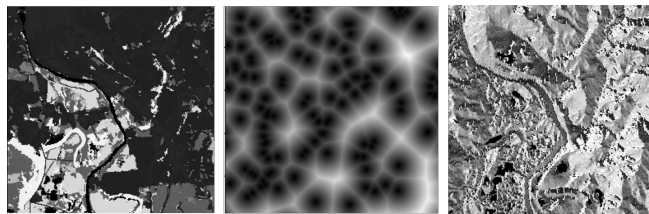


Figure 3: The figure shows three channels from a sample dataset: (1) the NLCD channel displaying land cover types, (2) the discharger proximity channel indicating proximity to the organic chemical manufacturing industries, and (3) the flow direction channel encoding upstream/downstream flows from physical modeling.

3.3 Ground Truth Masks

Our goal is to perform segmentation of surface water to predict PFAS contamination, but the available data consists of sparse point-level contamination measurements rather than dense labels. To generate dense training labels, we adopt a point-based ground truth expansion strategy, where every surface water pixel in a patch is labeled according to the EPA-defined contamination status of the patch’s sample point. Specifically, if the sample point indicates PFAS above the safety thresholds, all surface water pixels are labeled 1; if below, they are labeled 0. Non-surface water pixels are assigned a value of 2. This approach extends point-level data across the patch, assuming that nearby areas share similar contamination levels.

3.4 Noise Masks

To quantify the confidence that a pixel’s label (either 0 or 1) is correct since we are expanding the ground truth data, we combined four key factors; proximity to PFAS dischargers, land cover type, distance to other sample points, and downstream flow, into a single probability value. Each factor contributed a portion of the final probability, reflecting domain-informed assumptions about which conditions most strongly indicate correct labeling.

The final contamination probability for each surface water pixel i is computed as:

$$p_{\text{final}} = \alpha_1 \cdot p_{\text{dischargers}} + \alpha_2 \cdot p_{\text{landcover}} + \alpha_3 \cdot p_{\text{sample.dist}} + \alpha_4 \cdot p_{\text{downstream}} \quad (1)$$

where $p_{\text{dischargers}}$, $p_{\text{landcover}}$, $p_{\text{sample.dist}}$, and $p_{\text{downstream}}$ represent the contamination probabilities derived from (i) proximity to PFAS dischargers, (ii) land cover type, (iii) distance to other sample points, and (iv) downstream flow, respectively. In the following paragraphs, we briefly describe each factor:

Proximity to PFAS Dischargers ($p_{\text{dischargers}}$) If a pixel’s label was 1, we applied an exponential decay function of distance, assigning higher probabilities to pixels closer to known dischargers. For pixels labeled 0, we inverted this logic so that being near a discharger lowered confidence in the 0 label.

Land Cover Type ($p_{\text{landcover}}$) For pixels labeled 1, surrounding urban or built-up areas received higher probabilities than forested regions, consistent with research linking PFAS to industrial zones [Dimitrakopoulou *et al.*, 2024]. Conversely, for 0-labeled pixels, surrounding undeveloped or forested land cover increased confidence in low contamination.

Proximity to Other Sample Points ($p_{\text{sample.dist}}$) Pixels closer to known sample points were assigned higher probabilities using an exponential decay function based on distance to each sample point in the patch.

Downstream Flow ($p_{\text{downstream}}$) If a pixel lies downstream of a sample point labeled 1, its probability for label 1 increases, and similarly for label 0. This flow direction channel was generated using ArcGIS Pro [ESRI, nd], a geographic information system (GIS) software used for spatial analysis, and environmental modeling. ArcGIS Pro enabled extraction

of flow direction patterns based on digital elevation models (DEMs) [Earth Science Data Systems, 2024], ensuring downstream influence was accurately represented in the probability calculation.

Based on discussions with domain experts and experimental validation (see supplementary material), we set the weights as $\alpha_1 = 0.4$, $\alpha_2 = 0.3$, $\alpha_3 = 0.2$, and $\alpha_4 = 0.1$. Pixels at verified sample points themselves are assigned a probability of 1, reflecting complete confidence in their correctness. For other pixels, by tailoring contributions based on whether the pixel’s label was 1 or 0, we created a confidence score that indicates how likely the label is to be correct. For instance, pixels labeled 1 that are far from dischargers or 0 in developed areas receive low probabilities, indicating uncertainty. These noise masks down-weight uncertain labels and emphasize high-confidence ones, thereby enhancing model robustness.

3.5 Model

Our framework, FOCUS, is inspired by the Prithvi architecture [Blumenfeld, 2023] and employs a masked autoencoder (MAE) approach for pretraining. Instead of relying on raw satellite imagery and Prithvi’s pretrained weights, we pre-train our model on derived geospatial data products (e.g., land cover), which offer more contextual information for capturing the environmental nuances critical to PFAS contamination prediction (see Section 4). This pretraining uses masked autoencoding with a mean squared error loss. The pretrained encoder is then fine-tuned with a dedicated decoder head for the downstream task of PFAS prediction, resulting in improved data efficiency and overall performance.

3.6 Loss Function

The loss function used in FOCUS combines the focal loss with noise mask weighting as follows:

$$\mathcal{L}_{\text{FOCUS}} = \frac{1}{N} \sum_{i=1}^N \mathcal{L}_{\text{focal}}(z_i, y_i) \cdot M_i, \quad (2)$$

$$\mathcal{L}_{\text{focal}}(z_i, y_i) = (1 - p_{y_i})^\gamma \cdot \mathcal{L}_{\text{CE}}(z_i, y_i), \quad (3)$$

$$\mathcal{L}_{\text{CE}}(z_i, y_i) = -\log \left(\frac{\exp(z_{i,y_i})}{\sum_j \exp(z_{i,j})} \right) \quad (4)$$

where N is the number of pixels, z_i and y_i are the predicted logits and true label for pixel i , respectively, M_i is the noise mask value for pixel i , and p_{y_i} is the predicted probability for the true label y_i . Here, z_{i,y_i} is the logit for the true class and j indexes all classes.

The parameter $\gamma = 2$ is used in the focal loss to focus on hard-to-classify examples, as this value showed the best performance in previous studies introducing focal loss [Lin *et al.*, 2018]. Notably, class weights to address dataset imbalance are directly incorporated into the cross-entropy loss (\mathcal{L}_{CE}), removing the need for an explicit alpha term in focal loss. By combining focal loss and noise mask weighting, the loss function addresses label noise and class imbalance while emphasizing high-confidence pixels during training.

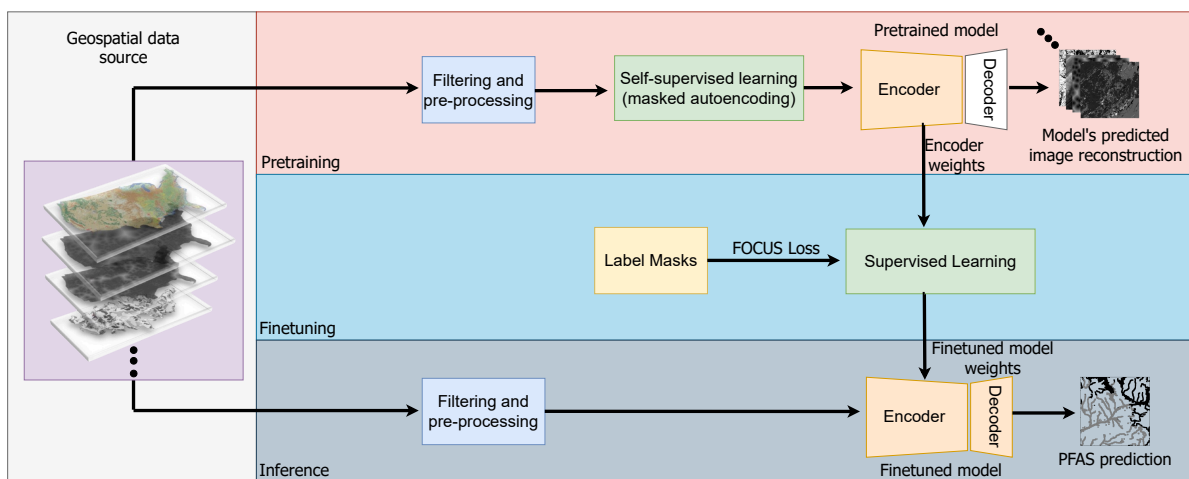


Figure 4: Model overview: high-level representation of FOCUS

3.7 Baselines

To contextualize our proposed framework for PFAS contamination prediction, we introduce several baseline approaches commonly employed in the field:

- **Pollutant transport simulation:** A process-based approach that models contaminant movement using hydrological principles.
- **Landsat-based method:** Uses Landsat 7 multispectral imagery [U.S. Geological Survey, nd] and the original Prithvi weights to infer contamination from raw satellite imagery.
- **FESTA loss approach:** An alternative state-of-the-art technique for sparse segmentation that encodes spatial and feature relationships, originally designed for datasets with mixed spatial formats such as incomplete lines, polygons, and points.
- **Kriging:** A geostatistical interpolation technique that predicts contamination based on spatial relationships between points.
- **Random forest:** Following the methodology of [DeLuca *et al.*, 2023], this model aggregates environmental features within a 5 km buffer around each sample from the NRSA dataset; for example, calculating the percentage of various land cover types and the distance to the nearest PFAS dischargers to predict contamination at individual points.
- **Rule-based approach:** This approach assigns contamination labels based on predefined environmental heuristics. Similar to our noise mask computation, but without data about ground truth points, it computes a contamination probability by combining weighted factors, such as discharger proximity, land cover, and flow direction, and then thresholds the result to yield binary labels.

Further details on Kriging and pollutant transport simulation are provided in the supplementary material. Collectively, these baselines provide a comprehensive benchmark for evaluating the performance and scalability of our proposed framework.

3.8 Experiments and Ablation Study

We now describe our experimental setup, with more details in the supplementary material.

Training Configuration. We adopted an 80%-20% split for each year’s data for training and testing, respectively, ensuring that the test set is geographically disjoint for rigorous evaluation. A batch size of 4 and a learning rate of 5×10^{-4} were adopted to preserve the stability of our pretrained backbone, minimizing the risk of large, destabilizing updates. In addition, we employed AdamW [Loshchilov and Hutter, 2019] as the optimizer with $\beta_1 = 0.9$ and $\beta_2 = 0.999$. Furthermore, we used a custom learning rate scheduler with an initial warmup phase followed by polynomial decay, which helped stabilize convergence and ensured that the model gradually adapted to the limited data.

Ablation Study. We conduct ablation studies across the following dimensions:

- **Raster Size:** To understand the influence of spatial context, we compare raster patches of 512×512 and 256×256 pixels. Larger patches capture broader contextual information, potentially including contamination sources farther from the sample point, while smaller patches reduce noise and focus on localized features. This evaluation identifies the trade-off between contextual richness and spatial precision.
- **Noise Weights:** We evaluate the impact of incorporating noise masks into the FOCUS loss function. With noise masks, pixel-wise confidence scores scale the focal loss to emphasize high-confidence pixels; without them, the loss reduces to the standard focal loss function [Lin *et al.*, 2018].

3.9 Metrics

The reported metrics include accuracy, Intersection over Union (IoU), F-score, precision, and recall. All the performance metrics in this study are reported exclusively from test set evaluations, using only the contamination points provided by the EPA datasets. These metrics provide a comprehensive

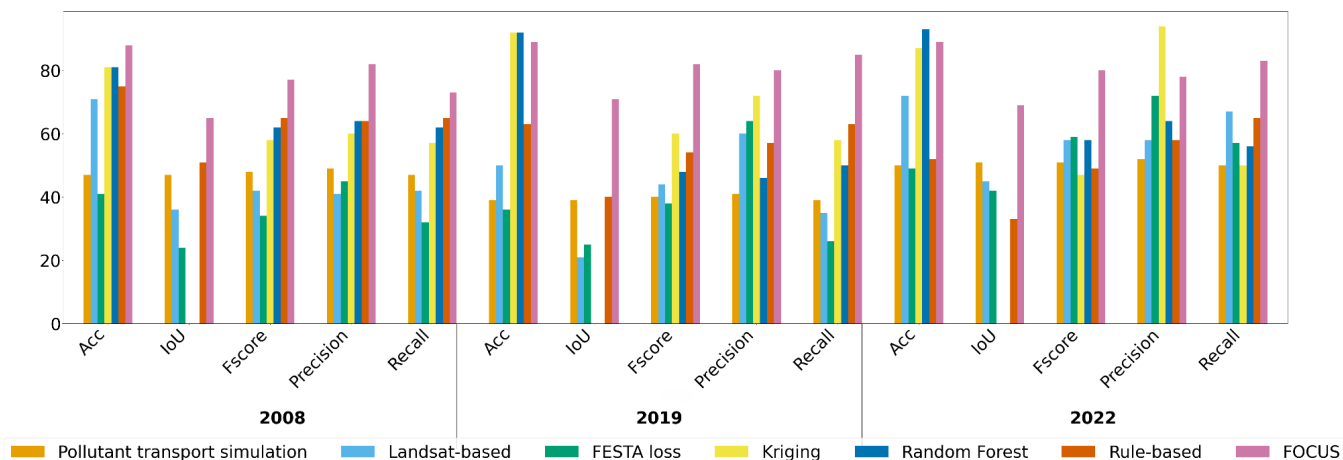


Figure 5: Comparison of performance across different methods and years.

evaluation of the model’s performance, where higher values indicate better performance: Accuracy captures overall correctness, IoU quantifies the overlap between predicted and ground truth contamination and is typically used for segmentation tasks, F-score balances the trade-off between precision and recall, precision indicates the model’s ability to correctly identify contamination without overestimating it (minimizing false positives), and recall measures its capacity to detect most contamination sites (minimizing false negatives). In addition, we assess timing efficiency as a metric to evaluate the model’s computational scalability. Together, these metrics provide a comprehensive evaluation of our model’s predictive effectiveness, spatial precision, and practical utility.

4 Results

All results in this section reflect performance on the test set, where evaluations are conducted solely on the actual contamination points from the EPA datasets.

We compared FOCUS against six alternative approaches for PFAS contamination prediction as shown in Figure 5. **Overall, FOCUS achieves better performance across all the years and most metrics**, aside from accuracy and precision in 2022. The Landsat-based method yielded moderate results, suggesting that geospatial data products are more effective for capturing PFAS contamination patterns than relying solely on raw satellite data. The Random Forest approach, despite achieving acceptable accuracy, suffered from lower F-score, precision, and recall, likely due to the limited spatial context from per-point feature aggregation. Similarly, although Kriging provided decent accuracy and precision, it struggled with recall, indicating difficulties in detecting all instances of contamination, and pollutant transport simulation demonstrated weak overall performance. The FESTA loss approach, originally tested on datasets with mixed spatial formats (e.g., incomplete lines, points, and polygons), showed suboptimal performance in our experiments as well. This may be attributed to our dataset’s exclusive use of point data and the complex dynamics of PFAS contamina-

tion, which may challenge the spatial continuity assumptions of the FESTA loss. While rule-based masks, designed to approximate contamination using domain-specific heuristics, can provide a reasonable estimate in some cases, they fall short in consistency and accuracy compared to the data-driven approach. This finding underscores the importance of incorporating domain expertise and AI for more reliable PFAS contamination prediction.

To further illustrate the model’s performance, we present a predicted contamination map using our model for a sample image in Figure 6. For this patch, real data was available only for the central pixel, corresponding to the location of an EPA sampling point. While the model correctly predicts contamination at this central point, its predictions for other surface water regions within the patch remain unverified due to no corresponding ground truth data. Further results on the model calibration as measured by the Expected Calibration Error [Guo *et al.*, 2017] are provided in the supplementary material.

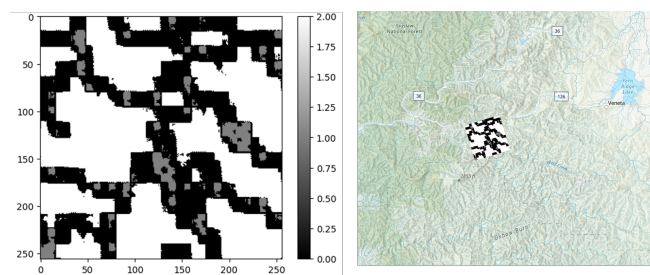


Figure 6: Left: Model-predicted contamination map for a 2019 patch; Right: Prediction overlaid on the U.S. map.

4.1 Ablation Results

Table 1 presents a comparison of three configurations: (i) point-based ground truth expansion masks using 256×256 pixels patches, (ii) point-based ground truth expansion masks using 512×512 pixels patches, and (iii) our FOCUS approach. The first two configurations employ standard focal loss, while

Metric	2008 (%)			2019 (%)			2022 (%)		
	256	512	FOCUS	256	512	FOCUS	256	512	FOCUS
Accuracy	84	75	88	87	85	89	78	78	89
IoU	61	52	65	68	66	71	57	56	69
F-score	73	67	77	80	78	82	71	71	80
Precision	75	66	82	77	76	80	70	70	78
Recall	71	72	73	84	83	85	87	84	83

Table 1: Comparison of performance across three approaches—256 × 256 pixels resolution, 512 × 512 pixels resolution, and FOCUS—over different years; bold values denote the best metric for each year.

FOCUS leverages noise masks to emphasize high-confidence pixels.

We observe that 256 × 256 patches generally perform as well as or better than 512 × 512 patches, likely because the smaller patch size reduces noise while preserving key spatial context. We did not evaluate patch sizes smaller than 256 × 256, consistent with literature indicating that excessively small patches can compromise accuracy and increase variability [Lechner *et al.*, 2009].

FOCUS extends standard focal loss by using noise masks to emphasize high-confidence pixels. As shown in Table 1, FOCUS consistently improves accuracy, IoU, F-score, and precision across all years. In 2008 and 2019, recall increases, whereas in 2022 it slightly decreases, indicating that FOCUS may sometimes favor precision over sensitivity. Overall, these results confirm that incorporating pixel-wise confidence through noise-based weighting enhances segmentation quality and model robustness.

4.2 Time Efficiency

	Feature extraction		Inference	
	ML	DL	ML	DL
For 1 km ² area	1.2 mins	4.7 sec	0.0003 sec	0.0005 sec
For NM	2 days	3.2 hrs	7.5 sec	13 sec

Table 2: Comparison of performance for feature extraction and inference using Random Forest and FOCUS over 1 km² area and Northern Michigan (NM).

We followed the methodology of DeLuca *et al.* [DeLuca *et al.*, 2023], which uses similar environmental features and the NRSA dataset with a Random Forest model, as a baseline for efficiency comparisons. Table 2 compares feature extraction and inference times between the ML method and our FOCUS approach over a 1 km² area and in Northern Michigan (NM).

For feature extraction, we aggregated environmental features within a 1 km buffer around each point for the ML method. On average, this per-point aggregation took about 1.2 minutes. In contrast, our deep learning approach processes the entire 1 km² patch, including the creation and stacking of individual raster channels, taking only 4.7 seconds on average. Over NM, ML extraction took about 2 days compared to 3.2 hours for our FOCUS approach.

For inference, the ML method took 0.0003 seconds per point (7.5 seconds for NM), while our FOCUS approach required 0.0005 seconds per patch (13 seconds for NM). Although FOCUS inference is marginally slower, this trade-off is acceptable given the efficiency gains in feature extraction and the advantage of producing dense, spatially contextualized predictions. All reported times for feature extraction over the 1 km² area and inference were averaged over 10 runs. Feature extraction for both methods was performed on an Intel Xeon Gold 6154 processor (3.0 GHz), while inference was conducted on an AMD Ryzen Threadripper PRO 7985WX processor, with an NVIDIA RTX 6000 Ada Generation GPU.

Overall, these results demonstrate that our deep learning framework offers a scalable and efficient solution for PFAS contamination mapping.

5 Conclusion and Future Work

PFAS contamination is a global environmental issue due to its persistence in water, soil, and wildlife. While methods like LC-MS offer high accuracy, they are expensive and slow. Alternative approaches, such as spatial interpolation, remote sensing, ML methods, and hydrological models, provide insights but struggle with feature engineering and loss of spatial context.

Our geospatial DL framework, incorporating the novel FOCUS loss, directly processes multi-channel raster data and integrates contextual information, improving detection accuracy and preserving spatial dependencies, making it a promising tool for large-scale PFAS contamination mapping that can help identify high-risk areas.

Future work will explore model uncertainty estimation to guide targeted sampling. This would enhance the robustness and reliability of our predictions. We plan to build on publicly available PFAS contamination maps, such as those produced by the Environmental Working Group [Environmental Working Group, 2024] and [U.S. Geological Survey, 2023], by deploying our AI-based framework responsibly.

Ethical Statement

The public dissemination of PFAS contamination maps carries significant ethical implications. Given the potential impact on public health, environmental justice, and even property values, it is essential to communicate our findings transparently and responsibly. Our interdisciplinary team met bi-weekly to discuss findings and collectively decide on next steps, ensuring that our approach remains well-informed and grounded in both technical rigor and community needs. Our framework is well-suited to also support the generation of visualizations that can reflect prediction uncertainty, thereby helping decision-makers and impacted communities make informed choices. Prior to deployment, we plan to engage local stakeholders and community groups via public forums and workshops to tailor our maps to community needs. This approach facilitates responsible use of the data and predictions in guiding remediation efforts and policy decisions.

References

- [Blumenfeld, 2023] Josh Blumenfeld. Nasa and ibm openly release geospatial ai foundation model for nasa earth observation data — earthdata, August 2023.
- [Bondi-Kelly *et al.*, 2023] Elizabeth Bondi-Kelly, Haipeng Chen, Christopher D. Golden, Nikhil Behari, and Milind Tambe. Predicting micronutrient deficiency with publicly available satellite data. *AI Magazine*, 44(1):30–40, 2023.
- [Breiman, 2001] Leo Breiman. Random forests. *Machine Learning*, 45(1):5–32, October 2001.
- [CDC, 2024] CDC. Centers for disease control and prevention, August 2024.
- [Chen and Guestrin, 2016] Tianqi Chen and Carlos Guestrin. Xgboost: A scalable tree boosting system. In *Proceedings of the 22nd ACM SIGKDD International Conference on Knowledge Discovery and Data Mining*, page 785–794, August 2016. arXiv:1603.02754 [cs].
- [Colorado Department of Public Health and Environment, nd] Colorado Department of Public Health and Environment. Pfas action plan, n.d.
- [Cong *et al.*, 2023] Yezhen Cong, Samar Khanna, Chenlin Meng, Patrick Liu, Erik Rozi, Yutong He, Marshall Burke, David B. Lobell, and Stefano Ermon. Satmae: Pre-training transformers for temporal and multi-spectral satellite imagery. (arXiv:2207.08051), January 2023. arXiv:2207.08051 [cs].
- [Crone *et al.*, 2019] Brian C. Crone, Thomas F. Speth, David G. Wahman, Samantha J. Smith, Gulizhaer Abulikemu, Eric J. Kleiner, and Jonathan G. Pressman. Occurrence of per- and polyfluoroalkyl substances (pfas) in source water and their treatment in drinking water. *Critical reviews in environmental science and technology*, 49(24):2359–2396, June 2019.
- [DeLuca *et al.*, 2023] Nicole M. DeLuca, Ashley Mullikin, Peter Brumm, Ana G. Rappold, and Elaine Cohen Hubal. Using geospatial data and random forest to predict pfas contamination in fish tissue in the columbia river basin, united states. *Environmental Science & Technology*, 57(37):14024–14035, sep 2023.
- [Dimitrakopoulou *et al.*, 2024] Maria-Eleni Dimitrakopoulou, Manos Karvounis, George Marinos, Zacharoula Theodorakopoulou, Eleni Aloizou, George Petsangourakis, Mihalis Papakonstantinou, and Giannis Stoitsis. Comprehensive analysis of pfas presence from environment to plate. *npj Science of Food*, 8(1):80, October 2024.
- [Doudrick, 2024] Kyle Doudrick. Removing pfas from public water will cost billions and take time • virginia mercury, April 2024.
- [Earth Science Data Systems, 2024] NASA Earth Science Data Systems. Digital elevation/terrain model (dem) — nasa earthdata, July 2024.
- [EcoCenter, nd] EcoCenter. Protecting communities from pfas pollution, n.d. PFAS contamination is one of the most pressing environmental health issues we face. These chemicals impact the lives and health of millions of Americans. Per- and polyfluoroalkyl substances (PFAS) are a class of more than 12,000 different chemicals with established links to adverse health impacts. There are more than 285 sites in Michigan that have been identified as PFAS contaminated, and in the United States that number is over 6,000.
- [Environmental Working Group, 2023] Environmental Working Group. Ewg study: Eating one freshwater fish equals a month of drinking water laced with pfos, January 2023. A new study by Environmental Working Group scientists finds that consumption of just a single serving of freshwater fish per year could be equal to a month of drinking water laced with the “forever chemical” PFOS at high levels that may be harmful.
- [Environmental Working Group, 2024] Environmental Working Group. Interactive map: Pfas contamination crisis: New data show 8,865 sites in 50 states, 2024.
- [ESRI, nd] ESRI. Desktop gis software — mapping analytics — arcgis pro, n.d.
- [GISGeography, 2017] GISGeography. Kriging interpolation - the prediction is strong in this one, February 2017.
- [Gokcesu and Gokcesu, 2021] Kaan Gokcesu and Hakan Gokcesu. Generalized huber loss for robust learning and its efficient minimization for a robust statistics. (arXiv:2108.12627), August 2021. arXiv:2108.12627 [stat].
- [Guo *et al.*, 2017] Chuan Guo, Geoff Pleiss, Yu Sun, and Kilian Q. Weinberger. On calibration of modern neural networks. (arXiv:1706.04599), August 2017. arXiv:1706.04599 [cs].
- [Hua *et al.*, 2022] Yuansheng Hua, Diego Marcos, Lichao Mou, Xiao Xiang Zhu, and Devis Tuia. Semantic segmentation of remote sensing images with sparse annotations. *IEEE Geoscience and Remote Sensing Letters*, 19:1–5, 2022. arXiv:2101.03492 [cs].
- [Kerner *et al.*, 2024] Hannah Kerner, Catherine Nakalembe, Adam Yang, Ivan Zvonkov, Ryan McWeeny, Gabriel Tseng, and Inbal Becker-Reshef. How accurate are existing land cover maps for agriculture in sub-saharan africa? *Scientific Data*, 11(1):486, May 2024.
- [kitorcoletti, 2012] kitorcoletti. What is modflow?, June 2012.
- [Langenbach and Wilson, 2021] Blake Langenbach and Mark Wilson. Per- and polyfluoroalkyl substances (pfas): Significance and considerations within the regulatory framework of the usa. *International Journal of Environmental Research and Public Health*, 18(21):11142, October 2021.
- [Largueche, 2006] Fatima-Zohra Benmost Largueche. Estimating soil contamination with kriging interpolation method. *American Journal of Applied Sciences*, 3(6):1894–1898, June 2006.

- [Lechner *et al.*, 2009] Alex Mark Lechner, Alfred Stein, Simon D. Jones, and Jelle Garke Ferwerda. Remote sensing of small and linear features: quantifying the effects of patch size and length, grid position and detectability on land cover mapping. *Remote Sensing of Environment*, 113(10):2194–2204, October 2009.
- [Li *et al.*, 2024] Xiongquan Li, Xukang Wang, Xuhesheng Chen, Yao Lu, Hongpeng Fu, and Ying Cheng Wu. Unlabeled data selection for active learning in image classification. *Scientific Reports*, 14(1):424, January 2024.
- [Liddie *et al.*, 2024] Jahred M. Liddie, Marie-Abèle Bind, Mahesh Karra, and Elsie M. Sunderland. County-level associations between drinking water pfas contamination and covid-19 mortality in the united states. *Journal of Exposure Science & Environmental Epidemiology*, page 1–8, October 2024.
- [Lin *et al.*, 2018] Tsung-Yi Lin, Priya Goyal, Ross Girshick, Kaiming He, and Piotr Dollár. Focal loss for dense object detection. (arXiv:1708.02002), February 2018. arXiv:1708.02002 [cs].
- [Loshchilov and Hutter, 2019] Ilya Loshchilov and Frank Hutter. Decoupled weight decay regularization. (arXiv:1711.05101), January 2019. arXiv:1711.05101 [cs].
- [Manz, 2024] Katherine E. Manz. Considerations for measurements of aggregate pfas exposure in precision environmental health. *ACS Measurement Science Au*, 4(6):620–628, December 2024.
- [Pelch *et al.*, 2022] Katherine E. Pelch, Anna Reade, Carol F. Kwiatkowski, Francheska M. Merced-Nieves, Haleigh Cavalier, Kim Schultz, Taylor Wolffe, and Julia Varshavsky. The pfas-tox database: A systematic evidence map of health studies on 29 per- and polyfluoroalkyl substances. *Environment International*, 167:107408, September 2022.
- [Reed *et al.*, 2015] Scott Reed, Honglak Lee, Dragomir Anguelov, Christian Szegedy, Dumitru Erhan, and Andrew Rabinovich. Training deep neural networks on noisy labels with bootstrapping. (arXiv:1412.6596), April 2015. arXiv:1412.6596 [cs].
- [Robinson *et al.*, 2020] Caleb Robinson, Anthony Ortiz, Kolya Malkin, Blake Elias, Andi Peng, Dan Morris, Bistra Dilkina, and Nebojsa Jojic. Human-machine collaboration for fast land cover mapping. *Proceedings of the AAAI Conference on Artificial Intelligence*, 34(0303):2509–2517, April 2020.
- [Salvatore *et al.*, 2022] Derrick Salvatore, Kira Mok, Kimberly K. Garrett, Grace Poudrier, Phil Brown, Linda S. Birnbaum, Gretta Goldenman, Mark F. Miller, Sharyle Patton, Maddy Poehlein, Julia Varshavsky, and Alissa Corder. Presumptive contamination: A new approach to pfas contamination based on likely sources. *Environmental Science & Technology Letters*, 9(11):983–990, nov 2022.
- [Schroeder *et al.*, 2021] Tim Schroeder, David Bond, and Janet Foley. Pfas soil and groundwater contamination via industrial airborne emission and land deposition in sw vermont and eastern new york state, usa. *Environmental Science. Processes & Impacts*, 23(2):291–301, March 2021.
- [Shoemaker and Tettenhorst, 2020] J. Shoemaker and D. Tettenhorst. Method 537.1 determination of selected per- and polyfluorinated alkyl substances in drinking water by solid phase extraction and liquid chromatography/tandem mass spectrometry (lc/ms/ms), 2020.
- [Sierra Club, nd] Sierra Club. Community science testing for pfas in water or biosolids, n.d. Community science to test for PFAS in rivers and lakes and in sludge/biosolids.
- [Singh and Verma, 2019] Prafull Singh and Pradipika Verma. *A Comparative Study of Spatial Interpolation Technique (IDW and Kriging) for Determining Groundwater Quality*, page 43–56. Elsevier, 2019.
- [SWAT, nd] SWAT. Soil & water assessment tool, n.d.
- [Tokranov *et al.*, 2023] Andrea K. Tokranov, Laura M. Bexfield, Katherine M. Ransom, James A. Kingsbury, Miranda S. Fram, Elise Watson, Danielle I. Dupuy, Stefan Voss, Bryant C. Jurgens, Paul E. Stackelberg, Delicia Beaty, and Kelly Smalling. Predictions of pfas in groundwater used as a source of drinking water and related data in the conterminous united states, 2023. Creative Commons Zero v1.0 Universal.
- [U.S. Environmental Protection Agency, nd] U.S. Environmental Protection Agency. Water pollution search — echo — us epa, n.d.
- [U.S. EPA, OW, 2015] U.S. EPA, OW. National rivers and streams assessment, June 2015.
- [U.S. EPA, 2024a] U.S. EPA. Contaminants to monitor in fish and shellfish advisory programs: Compilation of peer review-related information. 2024.
- [U.S. EPA, 2024b] OW U.S. EPA. 2020 great lakes human health fish fillet tissue study, apr 2024. Overviews and Factsheets.
- [U.S. Geological Survey, 2023] U.S. Geological Survey, May 2023.
- [U.S. Geological Survey, 2024] U.S. Geological Survey. National land cover database — u.s. geological survey, 2024.
- [U.S. Geological Survey, nd] U.S. Geological Survey. Landsat 7 level 2, collection 2, tier 1 — earth engine data catalog, n.d.
- [Zhang and Sabuncu, 2018] Zhilu Zhang and Mert R. Sabuncu. Generalized cross entropy loss for training deep neural networks with noisy labels. (arXiv:1805.07836), November 2018. arXiv:1805.07836 [cs].
- [Zhi *et al.*, 2024] Wei Zhi, Alison P Appling, Heather E Golden, Joel Podgorski, and Li Li. Deep learning for water quality. *Nature Water*, 2(3):228–241, 2024.

Supplementary Material

A Dataset

The dataset was curated to ensure that patches included in the training and testing sets were geographically disjoint, avoiding any overlap that could compromise the evaluation. Specifically, if multiple sample points were situated within the same patch, we selected a single patch containing all these points rather than creating multiple patches for each individual sample point. This avoided redundancy by reducing unnecessary duplication of spatial information. An illustration of this process is provided in Figure 7.

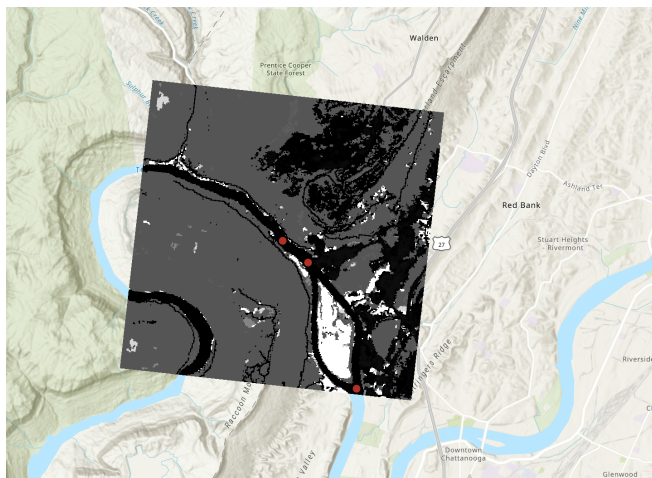


Figure 7: Example of patch selection for multiple sample points. The figure shows a single patch (outlined) overlaid on the U.S. map, with red points representing sample locations. Since all sample points are contained within the same patch, only this patch is added to the dataset, avoiding the creation of redundant patches centered around individual points.

In cases where two or more patches overlapped, as illustrated in Figure 8, all such patches were assigned to the same set (either training or testing). For example, if two patches partially shared the same geographic area, both patches were allocated to the training set or both to the testing set. This ensured that no part of a test patch had been seen during training, preserving the integrity of the evaluation

B Additional Results

We initially considered a conventional 70%-10%-20% split for training, validation, and testing, respectively, to facilitate intermediate performance monitoring. However, due to the limited availability of labeled data and a severe class imbalance with the minority class being particularly scarce, setting aside a separate validation set in order to guide the training process not only reduced the effective training size but also resulted in a highly skewed validation set. Through extensive empirical testing, we observed that a 80%-20% split for training and testing sets, respectively, significantly improved performance on the test set. This approach maximizes the data available for training while maintaining a rigorous, geographically disjoint evaluation on an independent test set. To assess the impact of allocating a separate validation set, we



Figure 8: Example of overlapping patch assignment. The figure illustrates two slightly overlapping patches overlaid on the U.S. map, each containing distinct sample points. To maintain disjoint training and testing sets, both patches are assigned to the same set (either training or testing), ensuring no part of a test patch overlaps with any patch seen during training.

compared the two dataset splits for training our model with focal loss: The conventional 70%-10%-20% split (training, validation, testing) versus the 80%-20% split (training and testing only). In our experiments here, we used only the standard focal loss without the additional noise-aware modifications to isolate the effect of the split on performance. Table 3 summarizes the performance metrics for each year under the two configurations.

Metric	2008 (%)		2019 (%)		2022 (%)	
	Val	W/o val	Val	W/o val	Val	W/o val
Accuracy	72	84	80	87	66	78
IoU	45	61	56	68	42	57
F-score	58	73	69	80	55	71
Precision	59	75	68	77	57	70
Recall	57	71	71	84	60	87

Table 3: Comparison of performance between models trained with and without a validation set (using focal loss) across different years.

Our experimental results indicate that the 80%-20% split, which allocates a larger portion of the data for training, consistently improves performance on the test set compared to the conventional split. This finding supports our decision to forgo a separate validation set for this task, given the limited data and severe class imbalance, and underscores the importance of maximizing training data for robust PFAS contamination prediction.

C Model Calibration

We evaluated model calibration using ECE, which quantifies the discrepancy between predicted probabilities and ob-

served outcomes where lower scores indicate better calibration. Table 4 shows the ECE scores for our model trained with FOCUS loss for the years 2008, 2019, and 2022.

Metric	2008	2019	2022
ECE Score	0.1	0.1	0.07

Table 4: ECE Scores for Models Trained with FOCUS Loss Across Different Years.

The very low ECE values, that is, 0.1 for 2008 and 2019, and 0.07 for 2022, demonstrate that our model’s predicted probabilities are closely aligned with the observed outcomes, indicating excellent calibration.

D Noise Mask Illustration

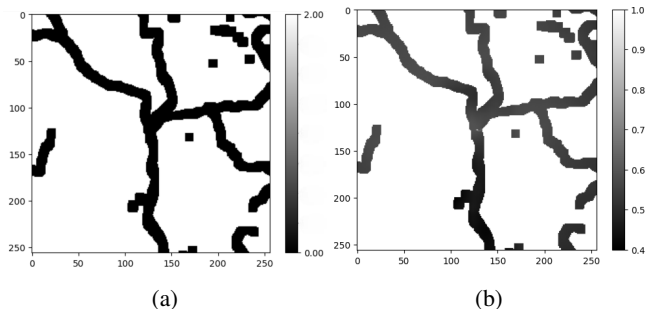


Figure 9: Illustration of a sample input mask and its corresponding noise mask: (a) the input mask assigns a label of 0 here to all surface water pixels (ground truth for PFAS contamination), and (b) the noise mask provides pixel-wise confidence scores. The model’s loss is computed as the focal loss between predictions and the input mask, scaled by the noise mask to emphasize high-confidence labels.

E Noise Mask Weights Ablation

Our ablation study on 2008 PFAS data compared several noise mask weight configurations. In Ablation 1, weights were set to 30% for dischargers, 40% for land cover, 20% for flow direction, and 10% for distance to sample points. Ablation 2 used 40% for dischargers, 30% for land cover, 20% for flow direction, and 10% for distance to sample points, while Ablation 3 applied 30% for dischargers, 40% for land cover, 10% for flow direction, and 20% for distance to sample points. Our current configuration, 40% dischargers, 30% land cover, 20% distance to sample points, and 10% flow direction, yielded the best overall performance, achieving the highest accuracy, IoU, F-score, and precision, even though recall was slightly lower. These results, in line with domain expert recommendations, confirm that our chosen configuration most effectively captures the critical environmental signals for PFAS contamination prediction.

F Kriging

We employed Kriging as a spatial interpolation technique to estimate PFAS (0 or 1). First, we examined the spatial structure of our data by calculating an empirical semivariogram.

Metric	Abl. 1	Abl. 2	Abl. 3	Current
Accuracy	84	81	81	88
IoU	61	60	60	65
F-score	73	73	73	77
Precision	75	71	71	82
Recall	71	76	76	73

Table 5: Comparison of performance across three noise weight ablations (Abl. 1, Abl. 2, and Abl. 3) and our current noise weight configuration.

Using latitude and longitude coordinates alongside the binary target variable, we computed pairwise distances and differences to produce a semivariogram plot, enabling us to observe how variance changed with increasing distance. This step informed the selection of appropriate variogram models (e.g., linear or spherical) for Kriging.

Next, we split the data on a state-by-state basis, ensuring geographic diversity between the training and testing subsets. We explored both Ordinary Kriging (assuming a stationary mean across the study area) and Universal Kriging (introducing a drift term to account for regional linear trends), but the two approaches produced essentially identical results on our dataset. After training each Kriging model on the geographic regions in the training set, we predicted PFAS presence at test set locations. Since we treated PFAS presence as a binary outcome, the resulting continuous Kriging predictions were thresholded at 0.5. We then computed standard classification metrics (such as precision, recall, and F1-score) to evaluate each model’s ability to distinguish between high contamination versus low contamination sites.

While Kriging provided a practical means of interpolating PFAS presence, its reliance on variogram assumptions and spatial stationarity can limit accuracy in areas with highly heterogeneous conditions. Nonetheless, the approach offered a useful baseline spatial model against which we compared our proposed DL framework, highlighting the value of more sophisticated spatial processes (e.g., hydrological connectivity) when modeling PFAS contamination.

G Pollutant Transport Simulation

Rather than running a simulation like SWAT directly, an often time-consuming and computationally intensive process due to its detailed process-based simulations of surface runoff, infiltration, evapotranspiration, and pollutant transport, we implemented a streamlined Python-based workflow. Frameworks like SWAT typically require extensive preprocessing of input data (e.g., delineating sub-basins, defining hydrologic response units, and calibrating numerous parameters) and can take hours or days to execute, particularly when modeling large numbers of small patches. By handling infiltration, runoff, and flow direction in a custom script, we can batch-process multiple patches more efficiently while still capturing essential pollutant movement patterns. While our simulation remains an approximation relative to a fully process-based model like SWAT, it provides a practical and computationally feasible alternative for investigating pollutant transport

in many geographically dispersed areas.

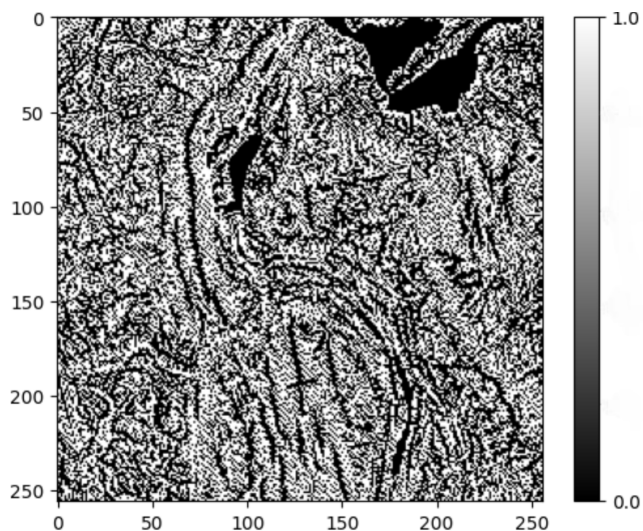


Figure 10: Example binary output from the pollutant transport simulation: 0 represents low contamination, and 1 represents high contamination. The simulation approximates the distribution of PFAS contamination based on hydrological and environmental parameters, providing a practical alternative to full-scale SWAT simulations.

First, we assign initial pollutant concentrations in each patch by setting cells flagged as “dischargers” to a high baseline value (e.g., 100), while land cover-based default concentrations provide moderately-low to low initial contamination levels for other cells. We then construct a Hydrologic Response Unit (HRU) parameter table that assigns infiltration and runoff values based on a cell’s land cover, soil type, and slope. Using these parameters, each patch’s land cover and soil rasters define infiltration/runoff ratios for every grid cell. We incorporate two key rasters; flow direction and flow accumulation, both exported from System for Automated Geoscientific Analyses (SAGA); a GIS and geospatial analysis tool focused on geospatial data processing, analysis, and visualization, to specify how water and pollutant mass move downstream. In each iteration, a fraction of the pollutant mass in each cell is transferred to its downstream neighbor according to the cell’s infiltration/runoff factors, guided by the flow direction raster and scaled by the flow accumulation values. Repeating this process causes pollutant mass to concentrate in lower-lying or higher-flow cells, thereby modeling how contamination evolves over time within the patch.

After the simulation converges, we produce a final pollutant concentration raster, thresholded by the median value of concentrations across all patches for the year to generate a binary contamination maps, as illustrated in Figure 10. The binary outputs, with values of 0 and 1 representing low and high contamination respectively, visualizes the simulation’s predictions of contamination distribution. These outputs are compared against test set patches containing actual observed PFAS presence to evaluate how accurately the simulation captures observed contamination patterns. Although this standalone approach remains computationally non-trivial, it is

more tractable for batch processing of multiple patches than running a full SWAT project repeatedly. Consequently, it provides a practical baseline for pollutant transport modeling within our broader framework, allowing us to compare simulated outputs to both real-world data and other modeling approaches.